Extended Kohler's Rule of Magnetoresistance

Extended Kohler's Rule of Magnetoresistance

Jing Xu,[1,2,*] Fei Han,[3,*] Ting-Ting Wang,[4,*] Laxman R. Thoutam,[1,5] Samuel E. Pate,[1,6] Mingda Li,[3,†] Xufeng Zhang,[2] Yong-Lei Wang,[4,‡] Roxanna Fotovat,[1] Ulrich Welp,[1] Xiuquan Zhou,[1] Wai-Kwong Kwok,[1] Duck Young Chung,[1] Mercouri G. Kanatzidis,[1,7] and Zhi-Li Xiao[1,6,§]

[1]*Materials Science Division, Argonne National Laboratory, Argonne, Illinois 60439, USA*
[2]*Center for Nanoscale Materials, Argonne National Laboratory, Argonne, Illinois 60439, USA*
[3]*Department of Nuclear Science and Engineering, Massachusetts Institute of Technology, Cambridge, Massachusetts 02139, USA*
[4]*Research Institute of Superconductor Electronics, School of Electronic Science and Engineering, Nanjing University, Nanjing 210093, China*
[5]*Department of Electronics and Communications Engineering, SR University, Warangal Urban, Telangana 506371, India*
[6]*Department of Physics, Northern Illinois University, DeKalb, Illinois 60115, USA*
[7]*Department of Chemistry, Northwestern University, Evanston, Illinois 60208, USA*

(Received 10 June 2021; revised 17 August 2021; accepted 15 September 2021; published 10 November 2021)

A notable phenomenon in topological semimetals is the violation of Kohler's rule, which dictates that the magnetoresistance MR obeys a scaling behavior of $\mathrm{MR} = f(H/\rho_0)$, where $\mathrm{MR} = [\rho(H) - \rho_0]/\rho_0$ and H is the magnetic field, with $\rho(H)$ and ρ_0 being the resistivity at H and zero field, respectively. Here, we report a violation originating from thermally induced change in the carrier density. We find that the magnetoresistance of the Weyl semimetal TaP follows an extended Kohler's rule $\mathrm{MR} = f[H/(n_T\rho_0)]$, with n_T describing the temperature dependence of the carrier density. We show that n_T is associated with the Fermi level and the dispersion relation of the semimetal, providing a new way to reveal information on the electronic band structure. We offer a fundamental understanding of the violation and validity of Kohler's rule in terms of different temperature responses of n_T. We apply our extended Kohler's rule to $BaFe_2(As_{1-x}P_x)_2$ to settle a long-standing debate on the scaling behavior of the normal-state magnetoresistance of a superconductor, namely, $\mathrm{MR} \sim \tan^2\theta_H$, where θ_H is the Hall angle. We further validate the extended Kohler's rule and demonstrate its generality in a semiconductor, InSb, where the temperature-dependent carrier density can be reliably determined both theoretically and experimentally.

DOI: 10.1103/PhysRevX.11.041029

Subject Areas: Condensed Matter Physics
Materials Science

I. INTRODUCTION

The magnetic-field-induced resistance change is conventionally termed as magnetoresistance (MR) [1]. In 1938, Kohler [2] developed a rule to account for the magnetoresistances in metals. Kohler's rule states that the magnetoresistance MR should be a function of the ratio H/ρ_0 of the magnetic field H to the zero-field resistivity ρ_0. That is, the field dependence of the magnetoresistances should exhibit a scaling behavior of $\mathrm{MR} = f(H/\rho_0)$, where $\mathrm{MR} = [\rho(H) - \rho_0]/\rho_0$ with $\rho(H)$ and ρ_0 being the resistivity at H and zero field at a fixed temperature, respectively. Kohler's rule of the magnetoresistances has been observed in materials [3–15] beyond metals and, recently, has been extensively used to understand novel magnetoresistance behavior such as the "turn-on" temperature behavior of the magnetoresistance in topological materials [5–15]. Violations of Kohler's rule have been often reported [16–40] and used as evidence for phase transitions [16,17] or for emergent new physics [18–22]. Here, we explore Kohler's rule of magnetoresistances in Weyl semimetals, where both its validity [5,6,8] and violation [23–25,27,28] are reported, with the aim to uncover the role played by the inevitable thermally induced change in the density of carriers on the scaling behavior. We find that the magnetoresistance of the Weyl semimetal tantalum phosphide (TaP) follows an extended Kohler's rule $\mathrm{MR} = f[H/(n_T\rho_0)]$, where n_T describes the relative change induced by thermal excitation in the carrier density, with $n_T = 1$

*These authors contributed equally to this work.
†mingda@mit.edu
‡yongleiwang@nju.edu.cn
§xiao@anl.gov

denoting the original Kohler's rule. We outline an innovative approach to obtain n_T without knowing the values of the carrier density, providing a new way to probe the temperature dependence of the carrier density. We show that n_T is associated with the Fermi level and the dispersion relation, thereby revealing information on the electronic band structure. We offer a fundamental description of the violation and validity of Kohler's rule in terms of different temperature responses of n_T. In particular, Kohler's rule is expected to be violated in materials with low carrier density where a noticeable density change due to thermal excitation occurs, while Kohler's rule should hold in materials where the carrier density is high enough such that its thermally induced change is experimentally indiscernible. Furthermore, by investigating the scaling behavior of the normal-state magnetoresistance in superconducting $BaFe_2(As_{1-x}P_x)_2$ crystals, we demonstrate that our extended Kohler's rule can account for the scaling $MR \sim \tan^2\theta_H$ where θ_H is the Hall angle, which was first observed in cuprate superconductors $YBa_2Cu_3O_{7-\delta}$ and $La_2Sr_xCuO_4$ [18] and has led to a long-standing debate in describing the normal-state magnetoresistance of a superconductor [19–21,33–41]. We also demonstrate the generality of our extended Kohler's rule in an undoped narrow-gap semiconductor, indium antimonide (InSb). At high temperatures, InSb is a compensated two-band system with high-mobility electrons and low-mobility holes, enabling us to determine the carrier density via Hall measurements and use its temperature dependence to test the validity of the n_T term in our extended Kohler's rule.

II. MATERIALS AND METHODS

Data reported here are obtained from two TaP crystals (sample TP1 and sample TP2), two $BaFe_2(As_{1-x}P_x)_2$ crystals with $x = 0.25$ (sample PL) and $x = 0.5$ (sample PH), and one undoped InSb crystal (sample IS).

A. Preparation of samples

1. TaP

Centimeter-sized single crystals of TaP are grown using the vapor transport method in two steps. In the first step, 3 g of Ta (Beantown Chemical, 99.95%) and P (Beantown Chemical, 99.999%) powders are weighed, mixed, and ground in a glovebox. The mixed powders are sealed in an evacuated quartz tube which is subsequently heated to 700 °C and sintered for 20 h for a prereaction. In the second step, the obtained TaP powder along with 0.4 g of I_2 (Sigma Aldrich, ≥99.8%) are sealed in a new evacuated quartz tube and are subsequently placed in a two-zone furnace with zone temperatures of 900 °C and 950 °C, respectively. The crystal growth time is 14 days. Because of the very high electrical conductivity of TaP, it is difficult to carry out high-precision electrical measurements on the as-grown crystals. To increase the electrical resistance of the samples, we polish the crystals down to a thin slab along the c axis (thickness of tens of micrometers). Electrical leads are gold wires glued to the crystals using silver epoxy H20E.

2. $BaFe_2(As_{1-x}P_x)_2$

Crystals of $BaFe_2(As_{1-x}P_x)_2$ with doping levels of $x = 0.25$ and $x = 0.50$ are grown using the self-flux method [42]. High-purity flakes of Ba (99.99%, Aldrich) and powders of FeAs and FeP (homemade from Fe, As, and P, 99.99%, Aldrich) are thoroughly mixed and placed in an Al_2O_3 crucible, which is then sealed in an evacuated quartz tube under vacuum and placed in a Lindberg box furnace. Crystals of plate shapes with lateral dimensions up to 2 mm and thicknesses up to 200 μm are obtained by heating up to 1180 °C and then cooling down to 900 °C at a rate of 2 °C/ min. Electrical leads of gold wires with a diameter of 50 μm are attached to the crystals using silver epoxy H20E.

3. InSb

A crystal of 5 mm × 5 mm × 0.5 mm is purchased from the MTI corporation. It is subsequently cut into pieces with desired lateral dimensions. Gold pads approximately 100 nm thick are deposited on locations predefined using photolithography. Electrical leads are fabricated by attaching 50-μm-diameter gold wires to the pads with silver epoxy H20E.

B. Resistance measurements

We conduct resistance measurements to obtain both $R_{xx}(H)$ and $R_{xy}(H)$ curves at various fixed temperatures, enabling the calculation of the resistivities $\rho_{xx}(H) = R_{xx}wd/l$ and $\rho_{xy}(H) = R_{xy}d$, where w, d, and l are the width, thickness of the sample, and the separation between the voltage contacts, respectively. The magnetic field is applied along the c axis of the crystals. The magnetoresistance is defined as $MR = [\rho_{xx}(H) - \rho_0)]/\rho_0$, where $\rho_{xx}(H)$ and ρ_0 are the resistivities at a fixed temperature with and without the presence of a magnetic field, respectively. In some cases, we obtain $\rho_{xx}(T)$ curves from the measured $\rho_{xx}(H)$ curves at fixed temperatures to avoid nonequilibrium temperature effects. Data for TaP and InSb are obtained using the conventional four-probe dc electrical transport measurement technique, while those for $BaFe_2(As_{1-x}P_x)_2$ are obtained using a low-frequency lock-in method.

III. RESULTS AND DISCUSSION

A. Extended Kohler's rule of magnetoresistance in Weyl semimetal TaP

TaP is a transition-metal monophosphide considered as the first realization of a Weyl semimetal [43–46]. Figure 1(a) presents the typical magnetotransport behavior of the longitudinal resistivity $\rho_{xx}(H)$ of a TaP crystal (sample TP1). Since the temperature dependence of $\rho_{xx}(T)$ has often exhibited interesting magnetoresistance phenomena such as the turn-on temperature

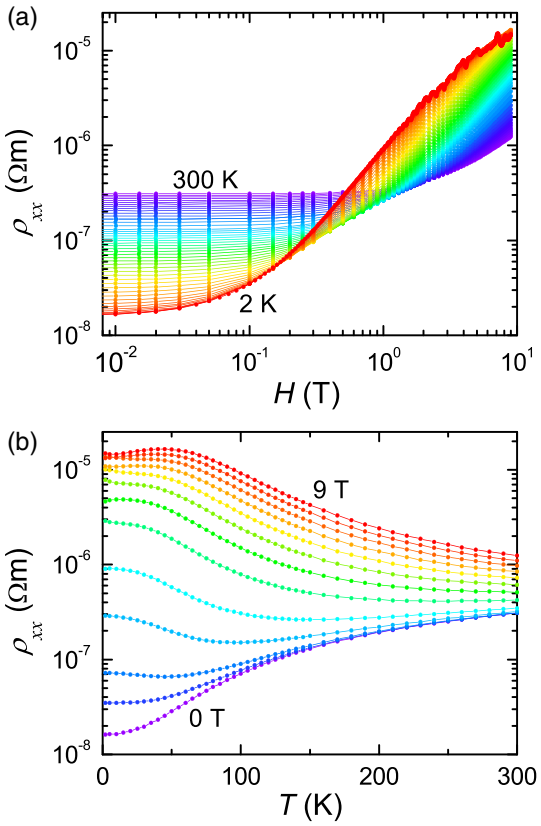

FIG. 1. Magnetoresistance of TaP. (a) Magnetic field dependence $\rho_{xx}(H)$ measured at temperatures of $T = 2$ K and from 5 to 150 K in intervals of 5 K and from 160 to 300 K in intervals of 10 K (from red to purple). (b) Temperature dependence $\rho_{xx}(T)$ constructed from $\rho_{xx}(H)$ in (a) at magnetic fields of $H = 0$, 0.1, 0.2, and 0.5 T and from 1 to 9 T in intervals of 1 T (from purple to red). The data are taken from sample TP1.

behavior [5,7,8] and topological insulating states [28–30], we also present $\rho_{xx}(T)$ curves in Fig. 1(b).

Both $\rho_{xx}(H)$ and $\rho_{xx}(T)$ in Fig. 1 are consistent with those reported recently in other materials with extremely large magnetoresistance [5–16,22–32]. The magnetoresistance MR can be as high as 10^5% at 2 K and 9 T [Fig. 2(a)] and follows the typical power law MR $\sim H^m$ behavior with $m \approx 1.6$ [dashed line in Fig. 2(c)] [27]. In the absence of a magnetic field, the resistivity decreases monotonically with temperature, as expected for a semimetal. When an external magnetic field is applied, the resistivity increases and a remarkable turn-on behavior appears in the $\rho_{xx}(T)$ curves: The temperature behavior of the resistivity changes from metal-like at high temperatures to insulatorlike at low temperatures at magnetic fields $H = 0.2$, 0.5, and 1.0 T and becomes insulatorlike over the entire temperature range at higher magnetic fields.

The key results of this work on TaP are displayed in Fig. 2, which presents the violation of Kohler's rule and highlights our extended Kohler's rule. For clarity, we present in Fig. 2(a) partial MR(H) curves derived from the $\rho_{xx}(H)$ data in Fig. 1(a), while all $\rho_{xx}(T)$ curves in Fig. 1(b) are used to obtain the MR(T) curves in Fig. 2(d). The respective scaling of MR(H) and MR(T) is presented in Figs. 2(b) and 2(e). Clearly, Kohler's rule MR $= f(H/\rho_0)$ is not followed in TaP, since the MR curves do not collapse onto a single curve when plotted against H/ρ_0. However, all curves in Fig. 2(b) are nearly in parallel with each other, suggesting that a single temperature-dependent multiplier to MR (y axis) or to H/ρ_0 (x axis) could cause them to overlap or collapse onto the same curve. Here, we tackle the latter case and uncover the underlying physics.

For the convenience of the forthcoming discussions, we designate $1/n_T$ as the temperature-dependent multiplier to H/ρ_0 (x axis) in the MR $\sim H/\rho_0$ curves in Fig. 2(b). In practice, we scale all the MR curves to the $T = 300$ K curve [i.e., $n_T = 1$ for MR(300 K) $\sim (1/n_T)(H/\rho_0)$] by varying n_T for each curve. As shown in Fig. 2(c), all curves in Fig. 2(b) indeed collapse onto the $T = 300$ K curve when the data are scaled as MR $\sim H/(n_T\rho_0)$. The n_T values for the MR $\sim H/\rho_0$ curves at various temperatures are presented in Fig. 3. It decreases monotonically from $n_T = 1$ at $T = 300$ K to $n_T = 0.45$ at $T = 2$ K. As presented in Fig. 2(f), we also account for the violation of Kohler's rule in Fig. 2(e) for the MR(T) curves by using the same n_T values as those used in Fig. 2(c). We find nearly identical behavior for the second TaP crystal (sample TP2), as demonstrated by the plots of MR $\sim H/(n_T\rho_0)$ in Fig. S1 [47], with n_T presented in Fig. 3. That is, the magnetoresistance of TaP follows an extended Kohler's rule with a thermal factor n_T:

$$\mathrm{MR} = f[H/(n_T\rho_0)]. \tag{1}$$

In the analysis above, we purposely use n_T in the denominator to couple with ρ_0 in Eq. (1), aiming to reveal the possible role of the carrier density in the violation of Kohler's rule. In a theoretical consideration on the violation of Kohler's rule in the normal-state resistivity of cuprate superconductors, Luo and Miley [41] introduce a MR scaling form (it is called a modified Kohler's rule) MR $= f(H\tau)$, where τ is the relaxation time of the carriers, since H and τ are coupled together as $H\tau$ for MRs in the derived equations [41]. Using $\rho_0 = m^*/(ne^2\tau)$, $H\tau$ can be expressed as $H\tau = (m^*/e^2)H/(n\rho_0)$, indicating that a scaling behavior of MR $= f[H/(n\rho_0)]$ is expected if m^* is temperature independent. However, there is no reliable way to obtain the values of n in a semimetal from transport measurements, as demonstrated in Fig. S2 [47] for n_H/n in a compensated system with $n_e = n_h = n$, where n_H is the density obtained from Hall effect measurements and in Fig. S3 [47] for electron and hole density derived from a two-band model analysis in TaP. Furthermore, m^* can change with temperature [48]. More importantly, materials such as multiband semimetals, where violation of Kohler's

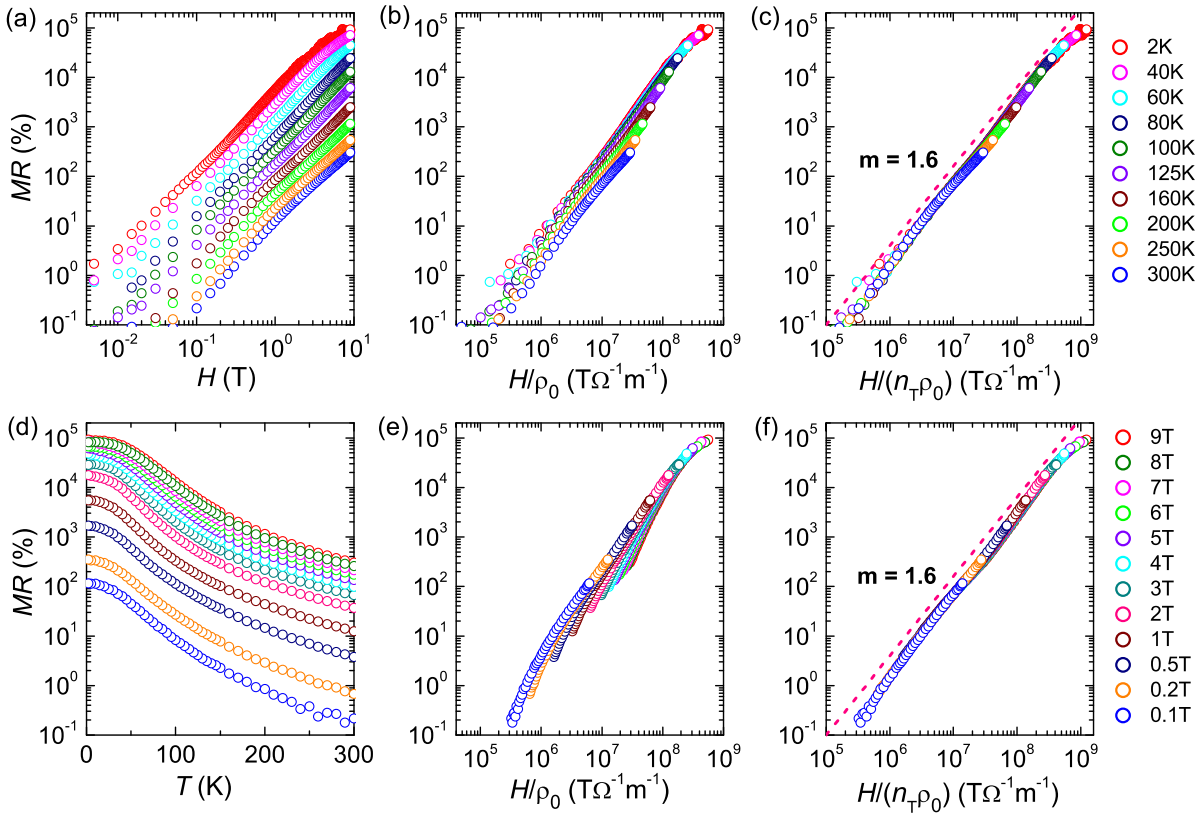

FIG. 2. Extended Kohler's rule of the magnetoresistance in TaP (sample TP1). (a),(d) Magnetic field and temperature dependences of the MR derived from data in Figs. 1(a) and 1(b), respectively. For clarity, (a) presents only partial MR(H) curves derived from the $\rho_{xx}(H)$ data in Fig. 1(a). (b),(e) Kohler's rule plots of the data in (a) and (d), respectively. (c),(f) Extended Kohler's rule plots of the MR curves in (a) and (d), respectively. The legends for (a)–(c) are on the top right, while legends for (d)–(f) are on the bottom right.

rule is reported, go beyond the (isotropic) single-band consideration in MR $= f(H\tau)$. We reveal in the discussion below that H and the mobility $\mu_i = e\tau/m_i^*$ $(i \geq 1)$ are interconnected as $H\mu_i$ in the MR expression. Also, it is the temperature-induced change in the carrier density that is responsible for the violation of Kohler's rule. Hence, our extended Kohler's rule expression in Eq. (1) provides a unique way to reveal the temperature dependence of the carrier density.

In the normal state of a cuprate superconductor, the temperature-induced change in the carrier density can be attributed to the existence of a pseudogap or Mott-Wannier excitons of weakly bound electrons and holes [41]. Differing from the linear temperature dependence of the carrier density used to explain the violation of Kohler's rule in cuprate superconductors [41], the n_T obtained in our samples can be approximately described by $n_T \sim T^2$ (Fig. S4 [47]), which can be attributed to the thermally induced change in the carrier density, as elaborated below.

As revealed by band structure calculations and angle-resolved photoemission spectroscopy (ARPES) experiments [43–46], TaP has a total of 12 pairs of Weyl nodes. Four of them, denoted as W1, are enclosed by an electronlike Fermi surface with energies below the Fermi level. The other eight pairs, denoted as W2, are enclosed by a holelike Fermi surface and with energies above the Fermi level. The band structure is illustrated in Fig. 3, with the relative locations of W1 and W2 with respect to the Fermi level, E_F. Considering the temperature-dependent Fermi-Dirac distribution, the total density of the conduction electrons at a given T can be straightforwardly obtained using

$$n = \sum_i \int_{E_i}^{\infty} g_i d\varepsilon / [1 + e^{(\varepsilon - E_F)/k_B T}], \tag{2}$$

where $i = 1$ and 2 correspond to Weyl nodes W1 and W2, respectively, with respective energies of $E_i = E_1$ and E_2. $g_i = g_1(\varepsilon)$ and $g_2(\varepsilon)$ are the density of states (DOS) for the conduction bands of W1 and W2, respectively. Since equal numbers of holes are created, Eq. (2) can also be used to calculate the thermally induced change in the hole density. In TaP, the densities of electron and holes are close to each other (Fig. S3c [47]). We focus only on electron density in the following discussions.

The energies E_1 and E_2 of the Weyl nodes W1 and W2 in TaP are determined by band structure calculations [44] and by ARPES measurements [45]. The theoretical DOS roughly follows $g \sim \varepsilon$ at ε up to approximately 0.3 eV

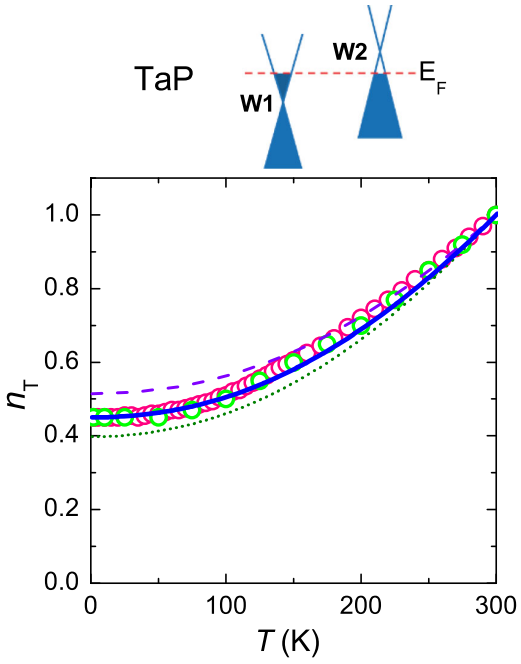

FIG. 3. Temperature dependence of n_T for samples TP1 (red circles) and TP2 (green circles) derived from the extended Kohler's rule Eq. (1). The dashed, solid, and dotted curves are calculated electron densities from Eq. (2) with energies (E_1 and E_2) (relative to the Fermi level) of the Weyl nodes W1 and W2 of (−53.1 meV, 19.6 meV), (−46.2 meV, 19.6 meV), and (−40 meV, 24 meV), respectively. To show the temperature dependence rather than their absolute values, all the calculated curves are normalized to the values at $T = 300$ K. Schematics of the electronic band structures are presented on the top of the panel.

and becomes nearly constant at higher energies [44,48]. As an estimate, we use $g_i = g_{i0}(\varepsilon - E_i)$ for $\varepsilon \leq 0.3$ eV and $g_i = g_{i0}(0.3 - E_i)$ for higher energies. In Fig. S5(a) [47], we present the calculated n_1 and n_2 and their sum n using the theoretical values of (−53.1 meV, 19.6 meV) for the energies (E_1, E_2) (relative to the Fermi level) of the Weyl nodes W1 and W2 and the electron and hole densities of $n_{e0} = 4.898 \times 10^{24}$ m^{-3} and $n_{h0} = 5.317 \times 10^{24}$ m^{-3} at $T = 0$ K [44]. As indicated by the dashed curve in Fig. 3, the total electron density n, normalized to the value at $T = 300$ K, describes the experimental n_T very well. The small deviation can be understood with sample-dependent (E_1, E_2), as demonstrated by the dotted curve obtained using the experimental values [45] of (−40 meV, 24 meV) and the solid curve calculated with (−46.2 meV, 19.6 meV), i.e., a slight increase in the theoretical E_1 value toward the experimental one while keeping the value of E_2 unchanged.

The above discussion indicates that the relative position of the Fermi level to the bottom of the conduction band and the top of the valence band, i.e., the density of electrons and holes at $T = 0$ K, affects the temperature dependence of n_T. As presented in Fig. S5(b) [47], the temperature-induced change in n_T mostly comes from the electron band. In Fig. S6(a) [47], we present n_T versus T curves calculated using different values of E_F in the electron band. It is clear that the sensitivity of n_T to T depends strongly on the Fermi level. In our TaP samples with $E_F \approx 50$ meV to the bottom of the conduction band, n_T nearly doubles when the temperature is increased from $T = 2$ to 300 K. However, it becomes challenging to experimentally resolve the change in n_T in the same temperature range when the Fermi level is increased to 200 meV. In this case, $n_T \approx 1$ and Kohler's rule should hold within experimental errors. Thus, the Fermi energy, i.e., electron density at $T = 0$ K, plays a key role in Kohler's rule. It directly explains why Kohler's rule is violated in type-I Weyl semimetals while it is upheld in their type-II counterparts, since the latter typically have much higher electron densities [5,6,8]. The validity of Kohler's rule in conventional metals is also not a surprise. They have much higher Fermi energies of a few eVs and electron densities of 10^{28-29} m^{-3} [49], which is 3–4 orders of magnitude higher than that of TaP, making thermally induced changes in the carrier density irrelevant. In Fig. S6 (b) [47], we show that the functional form of the DOS $g(\varepsilon)$ can further contribute to the n_T versus T relationship. When the exponent α in $g(\varepsilon) \sim \varepsilon^\alpha$ changes from $\alpha = 1$ for TaP to $\alpha = 1/2$ for typical metals, n_T becomes less sensitive to the change of T at the same Fermi level. This explains why the violation of Kohler's rule is observed more often in topological semimetals than in their trivial counterparts.

B. Extended Kohler's rule versus other alternative scaling forms of the magnetoresistance

In addition to topological materials, violations of Kohler's rule are often reported in cuprates and iron-based superconductors as well as other topologically trivial materials, and various alternative MR scaling forms have been introduced [18–20,33–41]. Among them, the most common one is

$$\mathrm{MR} = \gamma_H \tan^2 \theta_H, \tag{3}$$

where $\theta_H = \arctan(\rho_{xy}/\rho_{xx})$ is the Hall angle. This MR scaling behavior was first reported in cuprate superconductors, with $\gamma_H = 1.7$ and $\gamma_H = 1.5$–1.7 for underdoped and optimally doped $YBa_2Cu_3O_{7-\delta}$, respectively, and $\gamma_H = 13.6$ for $La_2Sr_xCuO_4$ [18]. It has numerous explanations [18–21,37–41] including the spin-charge separation scenario of the Luttinger liquid [21], current vertex corrections, and spin density wave [20]. Below, we show that the scaling Eq. (3) is a natural outcome of our extended Kohler's rule Eq. (1) in a compensated two-band material when the carrier mobility is very low, with γ_H being an indicator of the ratio of the hole and electron mobility. We also obtain similar scaling forms to Eqs. (1) and (3) for a low-mobility single-band system with an anisotropic Fermi

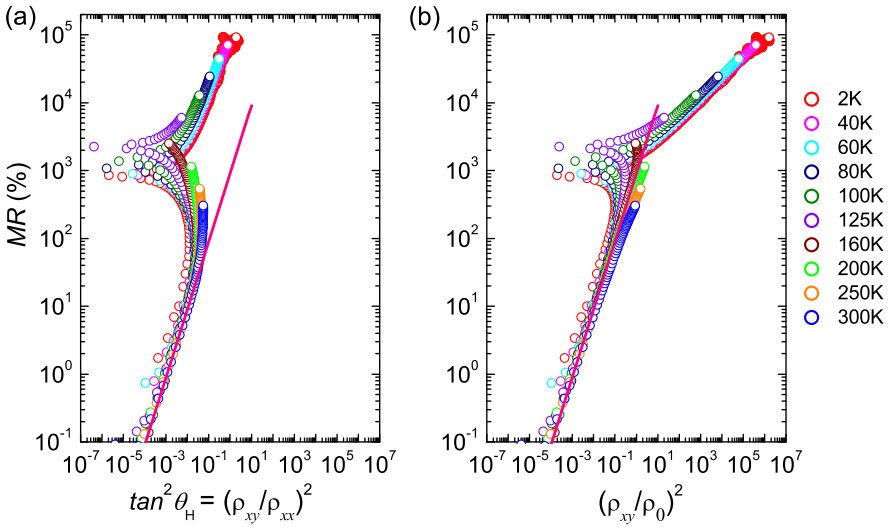

FIG. 4. Alternative scalings for the magnetoresistance in TaP (sample TP1) with Eqs. (3) (a) and (4) (b). The values of ρ_{xx}, ρ_0, and MR are taken from the same dataset as those used for the extended Kohler's rule in Figs. 2(a)–2(c) and the corresponding ρ_{xy} taken from Fig. S7(a) [47]. The solid pink lines in (a) and (b), respectively, represent $\mathrm{MR} = \gamma_H \tan^2\theta_H$ and $\mathrm{MR} = \gamma_H(\rho_{xy}/\rho_0)^2$ with $\gamma_H = 9$. The same colored open symbols are used in both panels.

surface as well as noncompensated two-band and multiband systems.

For a compensated two-band system where $n_e = n_h = n$, the second term in the denominator of Eq. (S1) [47] is zero, leading to $\mathrm{MR} = \mu_e\mu_h H^2$. Hence, MR can be rewritten as $\mathrm{MR} = \alpha_\mu/e^2[H/(n\rho_0)]^2$ where $\alpha_\mu = (\mu_h/\mu_e)/(1+\mu_h/\mu_e)^2$, $\rho_0 = [ne(\mu_h+\mu_e)]^{-1}$, and n_e, n_h, μ_e, and μ_h are the densities and mobilities of electron and holes, respectively. Thus, our extended Kohler's rule presented in Eq. (1) is valid if α_μ is temperature independent. Likewise, the second term in the numerator of Eq. (S2) [47] also becomes zero, yielding a linear Hall resistivity $\rho_{xy} = H(\mu_h/\mu_e - 1)/[en(\mu_h/\mu_e + 1)]$. Then, $\mathrm{MR} = \mu_e\mu_h H^2$ can be alternately expressed as

$$\mathrm{MR} = \gamma_H(\rho_{xy}/\rho_0)^2 \tag{4}$$

$$\text{with} \quad \gamma_H = (\mu_h/\mu_e)/(1-\mu_h/\mu_e)^2. \tag{5}$$

At very low mobilities, $\mathrm{MR} \to 0$ and $\rho_{xx} \approx \rho_0$, resulting in Eqs. (3) and (4) being equivalent. That is, in a compensated two-band system with very low mobilities, our extended Kohler's rule in Eq. (1) leads to the scaling behavior of Eq. (3).

The same conclusion can be reached for a nearly compensated two-band system, if the mobilities and/or the magnetic fields are low, such that the second term in the denominator of both Eqs. (S1) and (S2) [47] as well as the second term in the numerator of Eq. (S2) [47] become negligible. As revealed in TaP below, α_μ is indeed temperature insensitive [Fig. 5(b)]. Thus, our extended Kohler's rule Eq. (1) can be expressed as Eq. (3) for a compensated system as well as for a nearly compensated system with very low mobilities and/or at very low fields if the mobilities are high.

Underdoped $YBa_2Cu_3O_{7-\delta}$ [50,51] are indeed two-band materials. On the other hand, the optimal-doped $YBa_2Cu_3O_{7-\delta}$ (with $T_c = 90$ K) which also shows the scaling behavior akin to Eq. (3) is believed to be single-band system with an anisotropic Fermi surface [41]. As detailed in Supplemental Material [47], a single-band material would have no magnetoresistance if all carriers moving in the same direction have the same mobility. It exhibits magnetoresistance probably due to (i) the mobility distribution of carriers from different energy levels near the Fermi surface [1] and (ii) the existence of impurities. In the first case, we can obtain $\mathrm{MR} \approx \alpha^*_\mu[H/(n\rho_0)]^2$ [Eq. (S10) [47]] with $\alpha^*_\mu = 2\kappa/e^2[1 + (\mu_L/\mu_H)^2]/[1+\mu_L/\mu_H]^2$ [Eq. (S11) [47]] at low carrier mobilities such that $\mu_x^2H^2 \ll 1$, where μ_H and μ_L represent the highest and lowest mobility, respectively, of μ_x along the x direction and κ is the ratio (μ_y/μ_x) of the carrier mobilities μ_x and μ_y along the x and y directions. In the meantime, we can also obtain $\mathrm{MR} \approx \gamma^*_H\tan^2\theta_H$ with $\gamma^*_H = (9/8\kappa)[1 + (\mu_L/\mu_H)^2][1 - (\mu_L/\mu_H)^2]^2/[1 - (\mu_L/\mu_H)^3]^2$ [Eq. (S12) [47]. In the latter case, an optimal-doped $YBa_2Cu_3O_{7-\delta}$ crystal can be considered as a two-band or multiband system, with a dominating intrinsic anisotropic band together with one or more impurity bands. At low carrier mobilities, we have $\mathrm{MR} = [H/(n_T\rho_0)]^2$ [Eq. (S15) [47]] with $n_T = e[\sum_i(n_i\mu_i)]^{3/2}/[\sum_i(n_i\mu_i^3)]^{1/2}$ [Eq. (S16) [47] and $\mathrm{MR} \approx \gamma^{**}_H(\rho_{xy}/\rho_0)^2$ [Eq. (S17) [47]]

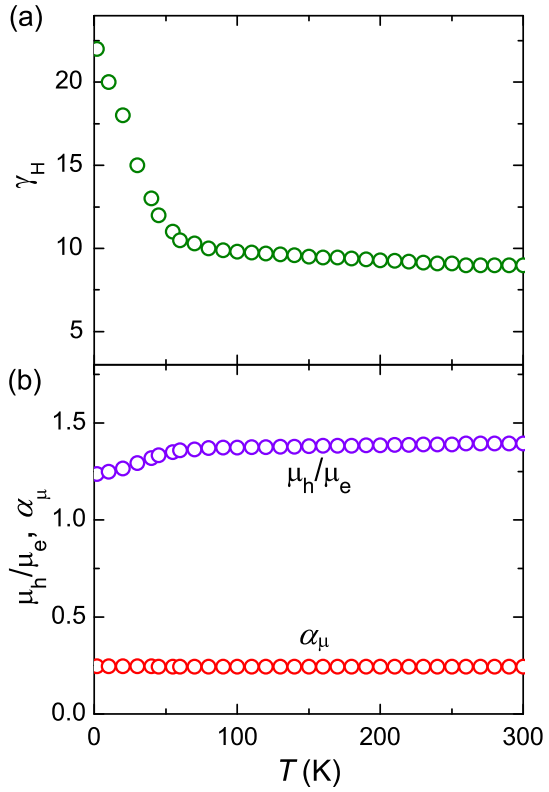

FIG. 5. Parameters derived from scaling magnetoresistances in Fig. 4(b) using Eq. (4). (a) Temperature dependence of γ_H, obtained at low magnetic fields from the plot of MR $\sim (\rho_{xy}/\rho_0)^2$. (b) The ratio μ_h/μ_e of the mobilities and the prefactor α_μ in MR $= \alpha_\mu/e^2[H/(n\rho_0)]^2$ at various temperatures, where μ_h/μ_e is calculated from Eq. (5) using the γ_H values in (a) and α_μ is obtained using $\alpha_\mu = (\mu_h/\mu_e)/(1+\mu_h/\mu_e)^2$.

with $\gamma_H^{**} = \sum_i(n_i\mu_i^3)\sum_i(n_i\mu_i)/[\sum_i(n_i\mu_i^2)]^2$, $\rho_0 = 1/\sum_i(en_i\mu_i)$, n_i and μ_i being the carrier density and mobility of the ith band. These results not only explain the observed scaling behavior of Eq. (3) in optimal-doped $YBa_2Cu_3O_{7-\delta}$, but also indicate that our extended Kohler's rule Eq. (1) should be valid whenever the scaling of Eq. (3) is observed.

TaP is a nearly compensated two-band system with high mobilities, as manifested by the large MRs [Fig. 2(a)] and nonlinear ρ_{xy} curves (Fig. S7 [47]). Thus, the scaling behavior in Eq. (3) is expected to fail when the MRs become significantly large, as confirmed by the plot in Fig. 4(a), which shows that Eq. (3) is roughly valid for MR $< 10\%$ and yields a value of $\gamma_H = 9$ at $T = 300$ K. On the other hand, Eq. (4) is an approximate expression of Eq. (1) at low magnetic fields and should be valid over a wider field range by avoiding the influence of $\rho_{xx}(H)$ in Eq. (3). As plotted in Fig. 4(b), MR $\sim (\rho_{xy}/\rho_0)^2$ indeed allows us to more reliably derive the γ_H values [Fig. 5(a)]. The corresponding μ_h/μ_e changes from 1.39 at $T = 300$ K to 1.24 at $T = 2$ K [Fig. 5(b)], leading to a nearly temperature-independent α_μ with a very small change ($<0.35\%$) from $T = 300$ K to $T = 2$ K [Fig. 5(b)].

In both Kohler's theory [2] and the derivations by Luo and Miley [41], $H\tau$ appears as a product that is inseparable in the expression for MR $= f(H\tau)$ and, hence, has been proposed as a modified Kohler's rule [33,36,41]. The magnetoresistances in the normal state of $La_{2-x}Sr_xCuO_4$ and $K_xFe_{2-y}Se_2$ single crystals are indeed found to follow the scaling behavior of MR $= f(H\tau)$ if $\tau \sim T^{-1}$ [33] and $\tau \sim T^{-2}$ [36] are, respectively, assumed. However, τ is not a parameter that can be conveniently obtained from resistivity measurements. As discussed in Sec. III. A, MR $= f(H\tau)$ does not consider the possible role of the carrier's effective mass and τ should be replaced with μ, which can have more than one value, as demonstrated in Eqs. (S10) and (S11) as well as Eqs. (S15) and (S16) [47]. Thus, its applications are limited, particularly for single-band systems with temperature-independent effective mass. It usually fails in two-band and multiband systems. For example, by assuming single relaxation time τ for all carriers, we can rewrite Eq. (S15) [47] as MR $= f(H\tau_T\tau)$ with $\tau_T = \sum_i(n_i/m_i^3)]^{1/2}/\sum_i(n_i/m_i)]^{1/2}$, where n_i and m_i are the carrier density and effective mass of the ith band, respectively. Clearly, τ_T will not be a constant when n_i and m_i are temperature dependent. That is, Eq. (1) extends the Kohler's rule to two-band and multiband systems, as experimentally confirmed by the MR scaling behavior in TaP. These derivations further indicate that n_T represents the temperature dependence of the carrier density in an anisotropic single-band system [$n_T \sim n$; see Eq. (S10) [47]] as well as in two-band and multiband systems [$n_T \sim f_n(T)$; see Eq. (S16) [47]] if the densities or mobilities from different bands have the same or similar temperature dependence, i.e., $n_i \approx n_i^0 f_n(T)$ and $\mu_i \approx \mu_i^0 f_\mu(T)$. In other cases, the thermal factor n_T in Eq. (1) contains contributions from the temperature dependences of the carrier densities and mobilities of all bands.

C. Generality of the extended Kohler's rule

1. Extended Kohler's rule of normal-state magnetoresistance in superconductor $BaFe_2(As_{1-x}P_x)_2$

The discussions in the preceding section indicate that Eq. (1), our extended Kohler's rule, applied to a semimetal also provides a sensible explanation for the alternative scaling rule presented in Eq. (3), which is used routinely to account for the normal-state magnetoresistances in several classes of superconductors [19–21,33–41]. Here, we experimentally confirm the applicability of Eq. (1) on two superconducting $BaFe_2(As_{1-x}P_x)_2$ crystals with $x = 0.25$ and 0.5, respectively. Their corresponding superconducting transition temperatures are 31 and 22 K, as revealed by the temperature dependence of the zero-field resistivity presented in Fig. S8 [47].

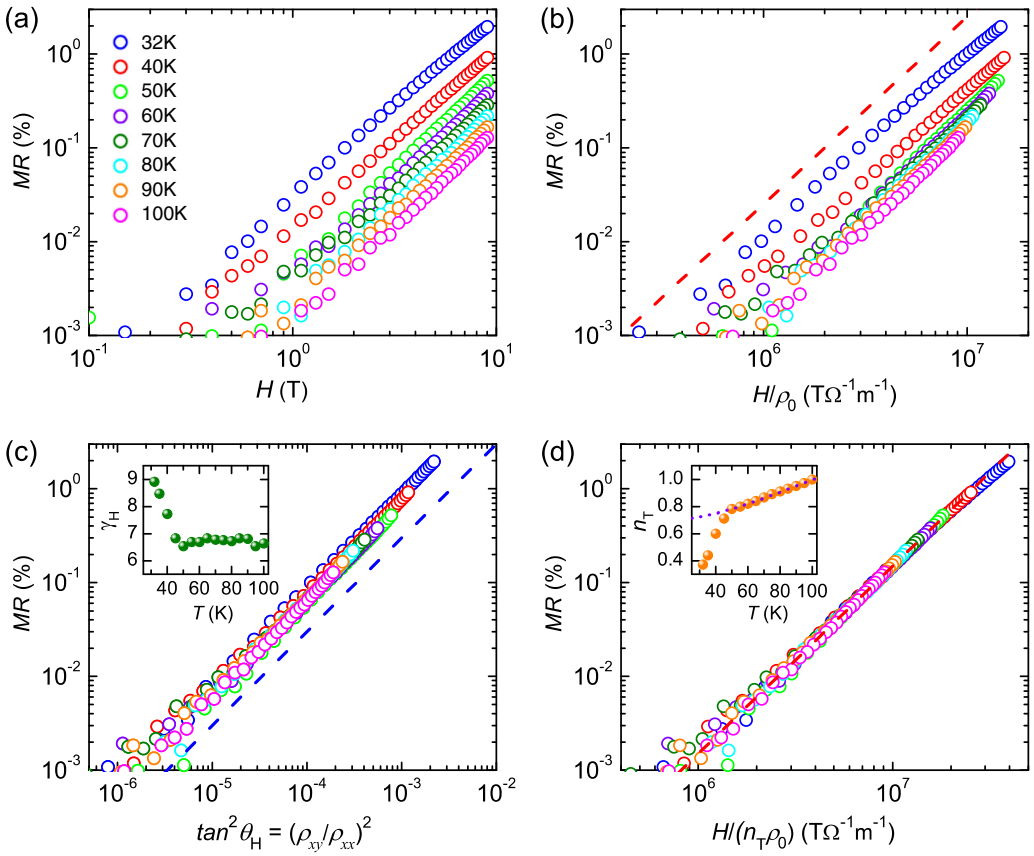

FIG. 6. Scaling behavior of the magnetoresistance of a $BaFe_2(As_{1-x}P_x)_2$ crystal with $x = 0.25$ (sample PL). (a) MR(H) curves at various temperatures. (b) Scaling according to the Kohler's rule. The red line represents MR $\sim (H/\rho_0)^2$. (c) Scaling according to Eq. (3). The dashed straight blue line is MR $= \gamma_H \tan^2\theta_H$ with $\gamma_H = 3$, demonstrating the validity of Eq. (3). The value of γ_H for each temperature is presented in the inset. (d) Scaling according to the extended Kohler's rule Eq. (1). The red line represents MR $\sim [H/(n_T\rho_0)]^2$. The inset shows the derived n_T, where the dotted purple line describes a possible pseudogap temperature behavior of $n_T = n_0 + \alpha T e^{-\Delta/k_B T}$ with $n_0 = 0.7$, $\alpha = 5.4 \times 10^{-3}$, and $\Delta = 5.18$ meV (or $\Delta/k_B = 60$ K). The same colored open symbols are used in all panels.

In the overdoped crystal with $x = 0.5$, we find that the magnetoresistance obeys Kohler's rule [Fig. S9(c) [47]], while the plot of MR versus $\tan^2\theta_H$ does not collapse the data into a single curve [Fig. S9(b)]. However, as indicated by the dashed magenta line, the MR versus $\tan^2\theta_H$ curves obtained at different temperature are indeed linear. The parallel shift in the log-log plot indicates that the prefactor γ_H in Eq. (3) is temperature dependent [inset in Fig. S9(b) [47]], similar to that found in TaP [Fig. 5(a)]. In the underdoped crystal with $x = 0.25$, we do observe both the violation of Kohler's rule [Fig. 6(b)] and the validity of the scaling Eq. (3) [Fig. 6(c)]. As indicated in Fig. 6(c) and the γ_H values in its inset, MR versus $\tan^2\theta_H$ curves at $T \geq 50$ K overlap each other, while those at $T < 45$ K show a slight parallel shift, with an increase of γ_H from approximately 7 at $T = 45$ K to approximately 9 at $T = 32$ K. In contrast, our extended Kohler's rule [Eq. (1)] works well over the entire temperature range as shown in Fig. 6(d). Similar to γ_H, the derived n_T [inset in Fig. 6(d)] also shows a significant change in its temperature dependence at $T \approx 50$ K. At $T \geq 50$ K, the temperature dependence of n_T is roughly linear. Interestingly, it can also be described by $n_T = n_0 + \alpha T e^{-\Delta/k_B T}$ [dashed line in the inset in Fig. 6(d) with $n_0 = 0.7$, $\alpha = 5.4 \times 10^{-3}$, and $\Delta = 5.18$ meV], analogous to the temperature dependence of the carrier density arising from carriers thermally excited over a pseudogap Δ in cuprates [52,53]. At $T \leq 45$ K, n_T changes with temperature at a much higher rate. The temperature (approximately 50 K) at which n_T changes its temperature sensitivity is coincident with that of a transition into an antiferromagnetic orthorhombic phase [35] (inset in Fig. S8 and discussion in its caption [47]). While further investigations are needed to account for the temperature behavior of n_T at temperatures above and below approximately 50 K, the results in Fig. 6 demonstrate that our extended Kohler's rule works when the scaling following Eq. (3) is obeyed. This provides experimental support for the conclusion in Sec. III. A that Eq. (1) can be expressed as Eq. (3) when the mobilities of the

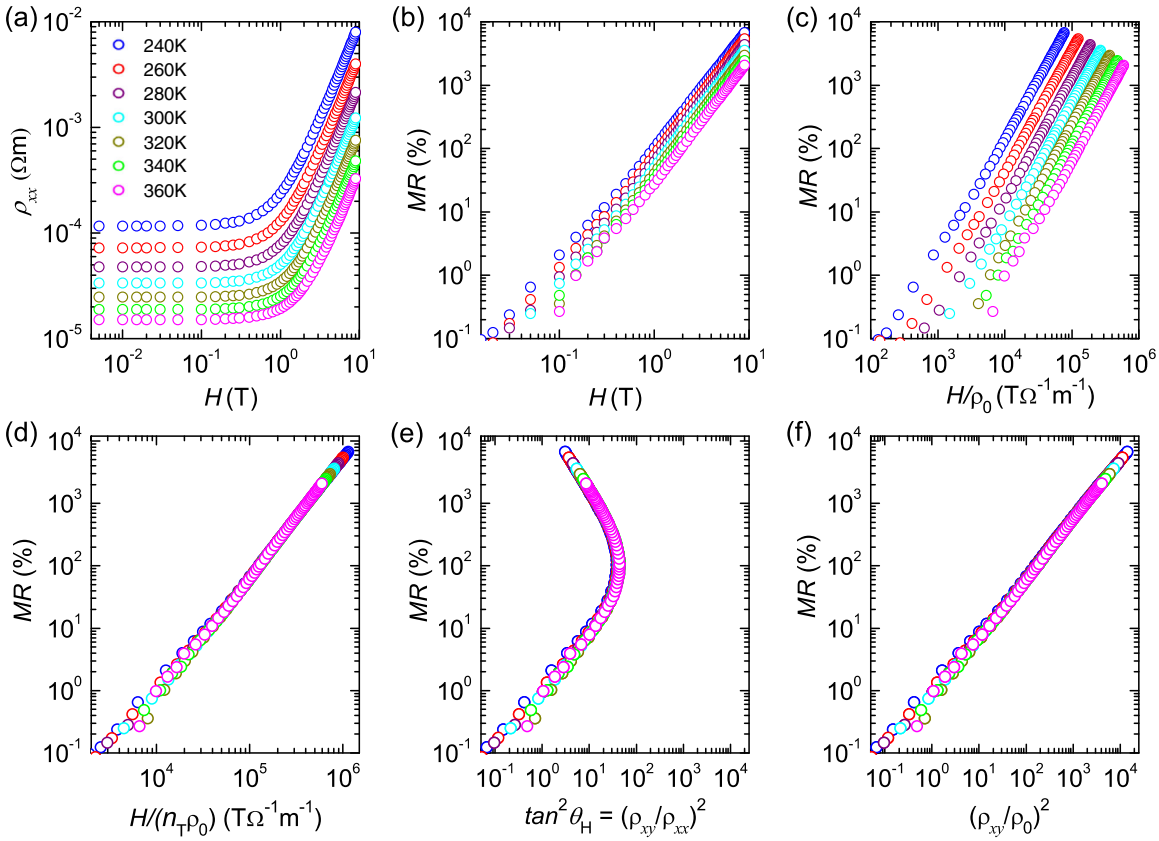

FIG. 7. Scaling behavior of the magnetoresistance in an InSb crystal (sample IS). (a) $\rho_{xx}(H)$ curves at various temperatures. (b) MR(H) curves at various temperatures. (c) Kohler's rule plot. (d) Scaling according to the extended Kohler's rule Eq. (1). (e),(f) Scaling according to Eqs. (3) and (4), respectively. The same colored open symbols are used in all panels.

carriers are low, which can be inferred from the negligible MRs in $BaFe_2(As_{1-x}P_x)_2$ (Fig. 6, up to 2% at $H = 9$ T). Furthermore, the above discussions show that n_T can be an indicator of a temperature-induced phase transition, if it exhibits a sudden change in the temperature sensitivity.

2. Extended Kohler's rule of magnetoresistance in semiconductor InSb

Following the discussions in Secs. III. A and III. B, it can be challenging to account for the temperature behavior of n_T derived from our extended Kohler's rule of Eq. (1) in semimetals and in the normal state of a superconductor. In the former case, one needs to know detailed information of the semimetal's electronic band structure that can be sample dependent [44,45]. In the normal state of a superconductor, n_T can be governed by more than one mechanism besides the electronic band structure, such as a pseudogap. In order to unambiguously validate the extended Kohler's rule of Eq. (1), we apply the scaling to the magnetoresistance of an undoped semiconductor. Kohler's rule is presumed to be violated due to the expected exponential temperature dependence of the intrinsic carrier density $n_i \sim T^{3/2}e^{-E_g/2k_BT}$ with E_g being the band gap [49], providing an exemplar system to showcase our extended Kohler's rule, Eq. (1). Its compensated nature also simplifies the analysis using Eqs. (S1) and (S2) [47] of the conventional two-band model, as discussed in Sec. III. A. We choose InSb, which is a narrow-gap semiconductor [54] with resistivities conveniently measurable at around room temperature [55]. Its temperature-dependent band gap E_g is available in the literature [54], enabling comparisons of the temperature dependence of n_T with that of the calculated n_i and/or of the reported band gap with that derived from n_T. Its large MR [55] (up to approximately 10^3% at $T > 250$ K) implies high carrier mobility, extending the range of the carrier mobility and enabling the validation of Eq. (4), from which scaling Eq. (3) is deduced at low carrier mobility. More importantly, we find a very large ($>10^2$) ratio (μ_e/μ_h) of the electron (μ_e) and hole (μ_h) mobility in InSb, where the carrier density n_i is practically the same as that (n_H) obtained from Hall measurements (Fig. S2 and caption [47]). This allows a further verification of n_T using the experimentally determined carrier density.

We present typical $\rho_{xx}(H)$ curves of InSb around room temperature in Fig. 7(a). We focus on data obtained at $T \geq 240$ K to avoid interference of quantum magnetoresistance that can occur at lower temperatures [55] and the contribution to the magnetoresistance by the residual impurity in

the nominally undoped crystal (Fig. S10 and caption [47]). As expected for a semiconductor, ρ_{xx} increases with decreasing temperature [also Fig. S10(a) [47]]. Figure 7(c) shows that Kohler's rule is violated in InSb. In fact, the curves in the Kohler's rule plot are separated from each other even further, compared to those prior to the scaling [Fig. 7(b)]. This is in contrast to those shown in Figs. 2(a) and 2(b) and in Figs. 6(a) and 6(b) for a semimetal (TaP) and for a superconductor [$BaFe_2(As_{2-x}P)_2$] in the normal state, because their zero-field resistivity ρ_0 has opposite temperature dependence to that of the semiconducting InSb. On the other hand, our extended Kohler's rule [Eq. (1)] can collapse all the data into a single curve [Fig. 7(d)]. The temperature dependence of the derived n_T can be well described theoretically [Fig. S11(b) [47]], unveiling band gaps comparable to those determined from other methods in the literature [inset in Fig. S11(b) [47]]. It is nearly indistinguishable to that of the experimental Hall carrier density n_H obtained from the $\rho_{xy}(H)$ curves [Fig. S11(a) [47]] as well as carrier density n_i [Fig. S12(c) [47]] obtained by simultaneous fittings of $\rho_{xx}(H)$ and $\rho_{xy}(H)$ curves using the two-band model [Fig. S12(a) [47]]. These results evidently prove the validity of our extended Kohler's rule Eq. (1) in semiconducting InSb, further demonstrating its generality. As presented in Fig. 7(e), a plot of MR versus $\tan^2\theta_H$ can also collapse all data into one common curve, which becomes, however, nonlinear with increasing magnetic field. This indicates that MR is not proportional to $\tan^2\theta_H$; i.e., the scaling provided by Eq. (3) is not valid. The reason is that Eq. (3) is deducible from Eq. (4) only when the carrier mobility is very low so that the magnetoresistance MR is negligible, i.e., $\rho_{xx}(H) \approx \rho_0$. On the other hand, Fig. 7(f) shows that the general form Eq. (4) does work well in InSb over the entire field range, confirming that in a compensated two-band system Eq. (4), i.e., $\mathrm{MR} = \gamma_H(\rho_{xy}/\rho_0)^2$, can be derived from the extended Kohler's rule Eq. (1), regardless of the value of the carrier mobility.

IV. CONCLUDING REMARKS

Since it was proposed more than 80 years ago for orbital magnetoresistances in nonmagnetic metals, Kohler's rule has been widely used to account for the magnetoresistance behavior in materials beyond simple metals, including cuprate and iron-based superconductors as well as in topological materials. On one hand, it offers a phenomenological understanding of novel magnetoresistance phenomena such as the turn-on temperature behavior of the magnetoresistance in topological materials. On the other hand, its violations have been often reported and attributed to temperature-induced phase transitions or other unconventional mechanisms. Stimulated by the widely reported violations of Kohler's rule in the newly discovered topological semimetals, we tackled the ubiquitous thermally induced changes in the carrier density. We used a low carrier density, type-I Weyl semimetal, TaP, to establish an extended Kohler's rule [Eq. (1)], which takes into account the role played by the temperature dependence of the carrier density. We demonstrated how the extended Kohler's rule naturally reduces to the original Kohler's rule in materials such as metals whose carrier density is so high that the temperature-induced change in it is experimentally indistinguishable. We applied our extended Kohler's rule to account for other alternative scaling forms of magnetoresistance, particularly the widely debated scaling behavior of $\mathrm{MR} \sim \tan^2\theta_H$ [Eq. (3)] discovered in cuprates and often applied to other superconductors. We showed that Eq. (3) can be deduced from our extended Kohler's rule Eq. (1) when the carrier mobility is very low. We also conducted measurements on the normal-state magnetoresistance in superconductor $BaFe_2(As_{1-x}P_x)_2$ to demonstrate that Eq. (1) is valid when the scaling Eq. (3) is observed. We further demonstrated the validation and generality of the extended Kohler's rule by investigating the magnetoresistance in a narrow-gap semiconductor, InSb, whose carrier density is expected to change strongly with temperature and can be determined both theoretically and experimentally.

Our extended Kohler's rule Eq. (1) offers a fundamental understanding of the violation and validity of Kohler's rule in terms of different temperature responses of the thermal factor n_T, with $n_T = 1$ denoting the original Kohler's rule. The results for TaP and InSb evidently show that n_T represents the temperature dependence of the carrier density, providing an alternative way to reveal information on the electronic band structure, e.g., Fermi level (in TaP) and band gap (in InSb). On the other hand, our extended Kohler's rule is inconclusive in understanding the temperature dependence of n_T in $BaFe_2(As_{1-x}P_x)_2$, which is a multiband system and where other mechanisms such as the pseudogap may also contribute to the thermally induced change in the carrier density. In general, we expect n_T to reflect the temperature dependence of the carrier density in (i) single-band (or one dominant band) systems and (ii) two-band and multiband materials whose carrier density and mobility in all bands have the same or similar temperature dependence, as demonstrated by the experimental results in the two-band systems TaP and InSb as well as the derived formulas of the compensated two-band systems and also noncompensated two-band and multiband materials. The temperature behavior of the thermal factor n_T depends on that of both carrier density and mobility, if a system with two or more bands has different temperature dependences for the carrier density and mobility in each band. In this case, detailed information of the carrier densities and mobilities of all bands is required to calculate n_T, making the comparison of theory and experiments more challenging. Further work on more materials is needed to ultimately

determine the limitations of our extended Kohler's rule. We note that other mechanisms can also cause violations of Kohler's rule. This work demonstrates that thermal effects on the carrier density and mobility may need to be considered before new mechanisms are proposed.

ACKNOWLEDGMENTS

Experimental design, magnetotransport measurements, and data analysis were supported by the U.S. Department of Energy, Office of Science, Basic Energy Sciences, Materials Sciences and Engineering. F. H. and M. L. acknowledge support DE-SC0020148 for supporting crystal growth. S. E. P., R. F., and Z.-L. X. received support by the National Science Foundation (Grant No. DMR-1901843). T.-T. W. and Y.-L. W. acknowledges support by the Jiangsu Excellent Young Scholar program (BK20200008) and the National Natural Science Foundation of China (61771235).

[1] J. M. Ziman, *Electrons and Phonons: The Theory of Transport Phenomena in Solids* (Cambridge University Press, Cambridge, United Kingdom, 2001).
[2] M. Kohler, *Zur Magnetischen Widerstandsänderung Reiner Metalle*, Ann. Phys. (Berlin) **424**, 211 (1938).
[3] L. Forro, K. Biljakovic, J. R. Cooper, and K. Bechgaard, *Magnetoresistance of the Organic Superconductor bis tetramethyltetraselenafulvalenium perchlorate [$(TMTSF)_2ClO_4$]: Kohler's Rule*, Phys. Rev. B **29**, 2839 (1984).
[4] M. K. Chan, M. J. Veit, C. J. Dorow, Y. Ge, Y. Li, W. Tabis, Y. Tang, X. Zhao, N. Barišić, and M. Greven, *In-Plane Magnetoresistance Obeys Kohler's Rule in the Pseudogap Phase of Cuprate Superconductors*, Phys. Rev. Lett. **113**, 177005 (2014).
[5] Y. L. Wang *et al.*, *Origin of the Turn-On Temperature Behavior in* WTe_2, Phys. Rev. B **92**, 180402(R) (2015).
[6] A. Narayanan *et al.*, *Linear Magnetoresistance Caused by Mobility Fluctuations in n-Doped* Cd_3As_2, Phys. Rev. Lett. **114**, 117201 (2015).
[7] F. Han *et al.*, *Separation of Electron and Hole Dynamics in the Semimetal LaSb*, Phys. Rev. B **96**, 125112 (2017).
[8] Q. L. Pei *et al.*, *Origin of the Turn-On Phenomenon in* Td-$MoTe_2$, Phys. Rev. B **96**, 075132 (2017).
[9] N. H. Jo *et al.*, *Extremely Large Magnetoresistance and Kohler's Rule in* $PdSn_4$*: A Complete Study of Thermodynamic, Transport, and Band-Structure Properties*, Phys. Rev. B **96**, 165145 (2017).
[10] J. Du *et al.*, *Extremely Large Magnetoresistance in the Topologically Trivial Semimetal* α-WP_2, Phys. Rev. B **97**, 245101 (2018).
[11] O. Pavlosiuk, P. Swatek, D. Kaczorowski, and P. Wiśniewski, *Magnetoresistance in LuBi and YBi Semimetals due to Nearly Perfect Carrier Compensation*, Phys. Rev. B **97**, 235132 (2018).
[12] Y. J. Hu, E. I. P. Aulestia, K. F. Tse, C. N. Kuo, J. Y. Zhu, C. S. Lue, K. T. Lai, and S. K. Goh, *Extremely Large Magnetoresistance and the Complete Determination of the Fermi Surface Topology in the Semimetal ScSb*, Phys. Rev. B **98**, 035133 (2018).
[13] A. I. U. Saleheen, R. Chapai, L. Xing, R. Nepal, D. Gong, X. Gui, W. Xie, D. P. Young, E. W. Plummer, and R. Jin, *Evidence for Topological Semimetallicity in a Chain-Compound* $TaSe_3$, npj Quantum Mater. **5**, 53 (2020).
[14] Q. Chen *et al.*, *Large Magnetoresistance and Nonzero Berry Phase in the Nodal-Line Semimetal* MoO_2, Phys. Rev. B **102**, 165133 (2020).
[15] R. Chapai, D. A. Browne, D. E. Graf, J. F. DiTusa, and R. Jin, *Quantum Oscillations with Angular Dependence in* $PdTe_2$ *Single Crystals*, J. Phys. Condens. Matter **33**, 035601 (2021).
[16] Y. Wu, N. H. Jo, M. Ochi, L. Huang, D. Mou, S. L. Bud'ko, P. C. Canfield, N. Trivedi, R. Arita, and A. Kaminski, *Temperature-Induced Lifshitz Transition in* WTe_2, Phys. Rev. Lett. **115**, 166602 (2015).
[17] S. Roßler, C. Koz, L. Jiao, U. K. Rossler, F. Steglich, U. Schwarz, and S. Wirth, *Emergence of an Incipient Ordering Mode in FeSe*, Phys. Rev. B **92**, 060505(R) (2015).
[18] J. M. Harris, Y. F. Yan, P. Matl, N. P. Ong, P. W. Anderson, T. Kimura, and K. Kitazawa, *Violation of Kohler's Rule in the Normal-State Magnetoresistance of* $YBa_2Cu_3O_{7-\delta}$ *and* $La_2Sr_xCuO_4$, Phys. Rev. Lett. **75**, 1391 (1995).
[19] A. Narduzzo, A. Enayati-Rad, S. Horii, and N. E. Hussey, *Possible Coexistence of Local Itinerancy and Global Localization in a Quasi-One-Dimensional Conductor*, Phys. Rev. Lett. **98**, 146601 (2007).
[20] H. Kontani, *Anomalous Transport Phenomena in Fermi Liquids with Strong Magnetic Fluctuations*, Rep. Prog. Phys. **71**, 026501 (2008).
[21] P. W. Anderson, *When the Electron Falls Apart*, Phys. Today **50**, No. 10, 42 (1997).
[22] X. Li *et al.*, *Pressure-Induced Phase Transitions and Superconductivity in a Black Phosphorus Single Crystal*, Proc. Natl. Acad. Sci. U.S.A. **115**, 9935 (2018).
[23] C.-L. Zhang, Z. Yuan, Q. D. Jiang, B. Tong, C. Zhang, X. C. Xie, and S. Jia, *Electron Scattering in Tantalum Monoarsenide*, Phys. Rev. B **95**, 085202 (2017).
[24] A. Wang, D. Graf, Y. Liu, Q. Du, J. Zheng, H. Lei, and C. Petrovic, *Large Magnetoresistance in the Type-II Weyl Semimetal* WP_2, Phys. Rev. B **96**, 121107(R) (2017).
[25] A. Wang, D. Graf, A. Stein, Y. Liu, W. Yin, and C. Petrovic, *Magnetotransport Properties of* MoP_2, Phys. Rev. B **96**, 195107 (2017).
[26] L.-L. Sun, Y.-Y. Wang, S. Xu, and T.-L. Xia, *Crystal Growth and Magneto-transport Properties of* α-$ZrSb_2$ *and* α-$HfSb_2$, Europhys. Lett. **120**, 37002 (2017).
[27] I. A. Leahy *et al.*, *Nonsaturating Large Magnetoresistance in Semimetals*, Proc. Natl. Acad. Sci. U.S.A. **115**, 10570 (2018).
[28] R. Sankar, G. Peramaiyan, I. P. Muthuselvam, S. Xu, M. Z. Hasan, and F. C. Chou, *Crystal Growth and Transport Properties of Weyl Semimetal TaAs*, J. Phys. Condens. Matter **30**, 015803 (2018).
[29] B. Qian *et al.*, *Extremely Large Magnetoresistance in the Nonmagnetic Semimetal YBi*, J. Mater. Chem. C **6**, 10020 (2018).

[30] V. Harimohan, A. Bharathi, R. Rajaraman, P. Magudapathy, C. David, and C. S. Sundar, *Magneto-resistance in Pristine and Irradiated* $TaAs_2$, AIP Adv. **9**, 045020 (2019).

[31] Q. Niu *et al.*, *Nonsaturating Large Magnetoresistance in the High Carrier Density Nonsymmorphic Metal CrP*, Phys. Rev. B **99**, 125126 (2019).

[32] A. Laha, S. Mardanya, B. Singh, H. Lin, A. Bansil, A. Agarwal, and Z. Hossain, *Magnetotransport Properties of the Topological Nodal-Line Semimetal CaCdSn*, Phys. Rev. B **102**, 035164 (2020).

[33] T. Kimura, S. Miyasaka, H. Takagi, K. Tamasaku, H. Eisaki, S. Uchida, K. Kitazawa, M. Hiroi, M. Sera, and N. Kobayashi, *In-Plane and Out-of-Plane Magnetoresistance in* $La_{2-x}Sr_xCuO_4$ *Single Crystals*, Phys. Rev. B **53**, 8733 (1996).

[34] P. Cheng, H. Yang, Y. Jia, L. Fang, X. Zhu, G. Mu, and H. H. Wen, *Hall Effect and Magnetoresistance in Single Crystals of* $NdFeAsO_{1-x}F_x$ *(*$x = 0$ *and 0.18)*, Phys. Rev. B **78**, 134508 (2008).

[35] S. Kasahara *et al.*, *Evolution from Non-Fermi- to Fermi-Liquid Transport via Isovalent Doping in* $BaFe_2(As_{1-x}P_x)_2$ *Superconductors*, Phys. Rev. B **81**, 184519 (2010).

[36] X. Ding, Y. Pan, H. Yang, and H. H. Wen, *Strong and Nonmonotonic Temperature Dependence of Hall Coefficient in Superconducting* $K_xFe_{2-y}Se_2$ *Single Crystals*, Phys. Rev. B **89**, 224515 (2014).

[37] S. Nair, S. Wirth, M. Nicklas, J. L. Sarrao, J. D. Thompson, Z. Fisk, and F. Steglich, *Precursor State to Unconventional Superconductivity in* $CeIrIn_5$, Phys. Rev. Lett. **100**, 137003 (2008).

[38] Y. Sun, T. Taen, T. Yamada, S. Pyon, T. Nishizaki, Z. Shi, and T. Tamegai, *Multiband Effects and Possible Dirac Fermions in* $Fe_{1+y}Te_{0.6}Se_{0.4}$, Phys. Rev. B **89**, 144512 (2014).

[39] R. Kumar, S. Singh, and S. Nair, *Scaling of Magnetotransport in the* $Ba(Fe_{1-x}Co_x)_2As_2$ *Series*, J. Phys. Condens. Matter **31**, 115601 (2019).

[40] N. Maksimovic, I. M. Hayes, V. Nagarajan, J. G. Analytis, A. E. Koshelev, J. Singleton, Y. Lee, and T. Schenkel, *Magnetoresistance Scaling and the Origin of H-Linear Resistivity in* $BaFe_2(As_{1-x}P_x)_2$, Phys. Rev. X **10**, 041062 (2020).

[41] N. Luo and G. H. Miley, *Kohler's Rule and Relaxation Rates in High-*T_c *Superconductors*, Physica (Amsterdam) **371C**, 259 (2002).

[42] C. Chaparro, L. Fang, H. Claus, A. Rydh, G. W. Crabtree, V. Stanev, W. K. Kwok, and U. Welp, *Doping Dependence of the Specific Heat of Single-Crystal* $BaFe_2(As_{1-x}P_x)_2$, Phys. Rev. B **85**, 184525 (2012).

[43] H. Weng, C. Fang, Z. Fang, B. A. Bernevig, and X. Dai, *Weyl Semimetal Phase in Noncentrosymmetric Transition-Metal Monophosphides*, Phys. Rev. X **5**, 011029 (2015).

[44] C.-C. Lee *et al.*, *Fermi Surface Interconnectivity and Topology in Weyl Fermion Semimetals TaAs, TaP, NbAs, and NbP*, Phys. Rev. B **92**, 235104 (2015).

[45] S. Y. Xu *et al.*, *Experimental Discovery of a Topological Weyl Semimetal State in TaP*, Sci. Adv. **1**, e1501092 (2015).

[46] Z. K. Liu *et al.*, *Evolution of the Fermi Surface of Weyl Semimetals in the Transition Metal Pnictide Family*, Nat. Mater. **15**, 27 (2016).

[47] See Supplemental Material at http://link.aps.org/supplemental/10.1103/PhysRevX.11.041029 for derivations of the scaling behavior of magnetoresistance in an anisotropic single-band system as well as a two-band or multiband system with low carrier mobility. It also includes (i) experimental data from sample TP2 and sample PH; (ii) additional data from sample TP1 and associated results from two-band model analysis; (iii) additional experimental data and analysis for sample IS; (iv) relationship between carrier density derived from the Hall effect measurements and the true carrier density in a compensated two-band system; and (v) effects of the Fermi level and dispersion relation on the temperature dependence of the thermal factor n_T in the extended Kohler's rule.

[48] S.-I. Kimura, H. Yokoyama, H. Watanabe, J. Sichelschmidt, V. Suss, M. Schmidt, and C. Felser, *Optical Signature of Weyl Electronic Structures in Tantalum Pnictides* TaP_n *(*$P_n = P$, As*)*, Phys. Rev. B **96**, 075119 (2017).

[49] C. Kittel, *Introduction to Solid State Physics*, 8th ed. (Wiley New York, 2004).

[50] S. E. Sebastian, N. Harrison, P. A. Goddard, M. M. Altarawneh, C. H. Mielke, R. Liang, D. A. Bonn, W. N. Hardy, O. K. Andersen, and G. G. Lonzarich, *Compensated Electron and Hole Pockets in an Underdoped High-*T_c *Superconductor*, Phys. Rev. B **81**, 214524 (2010).

[51] N. Doiron-Leyraud *et al.*, *Evidence for a Small Hole Pocket in the Fermi Surface of Underdoped* $YBa_2Cu_3O_y$, Nat. Commun. **6**, 6034 (2015).

[52] V. V. Kabanov, J. Demsar, B. Podobnik, and D. Mihailovic, *Quasiparticle Relaxation Dynamics in Superconductors with Different Gap Structures: Theory and Experiments on* $YBa_2Cu_3O_{7-\delta}$, Phys. Rev. B **59**, 1497 (1999).

[53] L. P. Gor'kov and G. B. Teitel'baum, *Interplay of Externally Doped and Thermally Activated Holes in* $La_{2-x}Sr_xCuO_4$ *and Their Impact on the Pseudogap Crossover*, Phys. Rev. Lett. **97**, 247003 (2006).

[54] C. L. Littler and D. G. Seiler, *Temperature Dependence of the Energy Gap of InSb Using Nonlinear Optical Techniques*, Appl. Phys. Lett. **46**, 986 (1985).

[55] J. S. Hu and T. F. Rosenbaum, *Classical and Quantum Routes to Linear Magnetoresistance*, Nat. Mater. **7**, 697 (2008).